Acta Crystallographica Section A
Foundations of Crystallography
ISSN 0108-7673

Received 29 November 2001
Accepted 18 March 2002

Structure of nanocrystalline anatase solved and refined from electron powder data[1]

T. E. Weirich,[a]* M. Winterer,[b] S. Seifried[b] and J. Mayer[a]

[a]Gemeinschaftslabor für Elektronenmikroskopie der Rheinisch-Westfälischen Technischen Hochschule Aachen, Ahornstrasse 55, D-52074 Aachen, Germany, and [b]Technische Universität Darmstadt, Fachbereich Material- und Geowissenschaften, Fachgebiet Dünne Schichten, Petersenstrasse 23, D-64287 Darmstadt, Germany. Correspondence e-mail: weirich@gfe.rwth-aachen.de

Energy-filtered Debye–Scherrer electron powder data have been successfully employed to determine the structure of nanocrystalline anatase (TiO_2). The performed structure analysis includes determining the unit cell, space group, solving the structure *via* direct methods from extracted intensities and refining the structure using the Rietveld technique. The refined structural parameters for space group $I4_1/amd$ are a = 3.872 (2), c = 9.616 (5) Å with titanium at 0.5, 0.75, 0.375 and oxygen at 0.5, 0.75, 0.1618 (6). The obtained structure indicates low internal stress as judged from the almost regular geometry of the TiO_6 building blocks. Striking resemblance with the anatase structure determined previously by Burdett, Hughbanks, Miller, Richardson & Smith [*J. Am. Chem. Soc.* (1987). **109**, 3639–3646] from neutron diffraction on coarse-grained material gives strong support for the correctness of the structure determined here. The result of the present study shows that the methods originally developed for determining structures from X-ray powder data work equally well with data from electron powder diffraction. This may open the window for structural investigations on the vast number of nanocrystalline materials and thin films whose structures are difficult to determine by X-ray diffraction since they are frequently only available in small quantities.

1. Introduction

Since the discovery of (transmission) electron diffraction by G. P. Thomson and A. Reid in 1927 (Thomson & Reid, 1927), it has always been very challenging to use electron data analogous to X-rays for determining crystal structures (*e.g.* Pinsker, 1953; Vainshtein, 1964; Zvyagin, 1967; Cowley, 1968; Vainshtein *et al.*, 1992). Despite the doubts that have been held for a long time against this approach, recent work on organic and inorganic materials proves that electron diffraction structure analysis is an independent method for accurate structure determination of materials too small in size to be investigated by single-crystal X-ray diffraction (*e.g.* Dorset, 1995; Zou *et al.*, 2000). However, whilst most of the earlier work deals with determining crystal structures from single-crystal or *oblique texture* patterns (Zvyagin, 1999), there was until recently very little effort to determine structures from non-textured electron powder data. The main reason why this is still a nearly unexplored field is related to problems that are encountered in any *ab initio* structure determination from powder data, *e.g.* difficulties in determining the unit cell, assignment of the correct space group and extraction of reliable intensities $I(hkl)$, which are needed to solve the structure (Cheetham, 1995). Nevertheless, the tremendous progress made during the last few years in determining structures from X-ray powder data (Giacovazzo, 1996; Harris & Tremayne, 1996) raises hope that these methods may also be used for *ab initio* structure determinations with electron powder data. In a previous study on nanocrystalline anatase (Weirich *et al.*, 2000), it was shown that 300 keV electron powder data can be employed for structure refinement with the Rietveld method (Young, 1995; Albinati & Willis, 1999). The present contribution describes the full structure determination of the same material from energy-filtered electron powder data with consequent application of the methods that were originally developed for the X-ray complement.

2. Sample

The investigated nanocrystalline TiO_2 powder [average particle size about 7 nm (Weirich *et al.*, 2000)] was synthesized *via* chemical vapour synthesis (CVS) from titanium tetra-isopropoxide and oxygen in a hot-wall reactor held at a temperature of 1200 K (Seifried *et al.*, 2000). The as-prepared powder was intimately dispersed in methanol and a standard

[1] Presented at the microsymposium on *Electron Crystallography of Small Molecules and Organic Materials*, 19th European Crystallographic Meeting, Nancy, France, 25–31 August 2000.

copper-grid-supported holey carbon film was loaded with a droplet of the prepared suspension and dried on air.

3. Methods and results

Energy-filtered Debye–Scherrer electron powder patterns from agglomerates that covered the holes of the carbon film were recorded on Fuji imaging plates using the Zeiss EM912-Ω transmission electron microscope at the Max-Planck Institut für Metallforschung in Stuttgart, Germany. The microscope was operated at 120 kV with a nominal zero-loss window of 10 eV. The digitized images (Fig. 1) were calibrated with a diffraction standard of nanocrystalline gold and quantified by the *ELD* program (Calidris, Sollentuna, Sweden). While conventional powder diffraction uses as input radially averaged intensity profiles, it turned out that employing radially integrated intensity profiles instead has significant advantages for determining the unit cell and solving the structure. The consequences of using radially integrated intensities will be discussed throughout the following description of the structure determination. Integrated intensities $I_{\rm int}(2\Theta)$ were obtained from the radially averaged intensities $I_{\rm rad}(2\Theta)$ using the relation (Weirich *et al.*, 2000):

$$I_{\rm int}(2\Theta) = 2\pi S G I_{\rm rad}(2\Theta),$$

G geometrical factor $\quad L$ camera length

$$G = L \sin 2\Theta / \cos\Theta \quad S \text{ scale factor.}$$

The used procedure of structure determination from electron powder data is basically the same as used in the X-ray case:

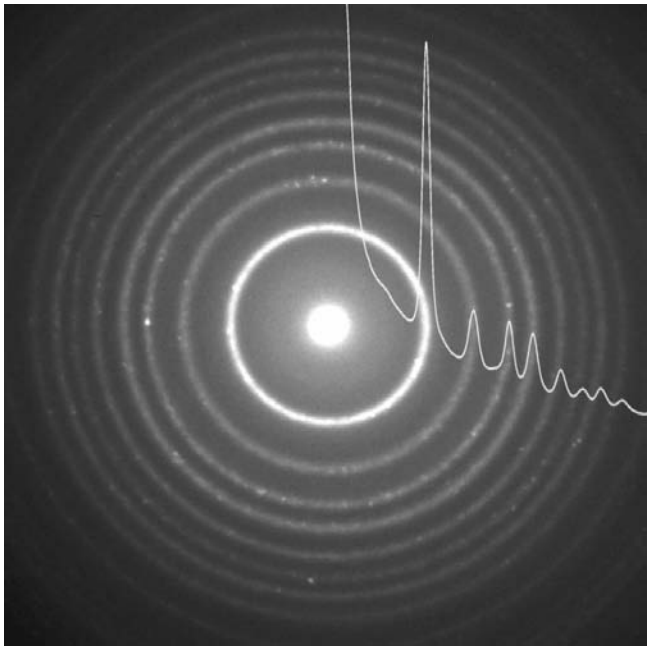

Figure 1
Experimental electron powder pattern of nanaocrystalline anatase (average crystal size about 7 nm) obtained with a Zeiss EM912 Ω-filter electron microscope on imaging plate (U = 120 kV, nominal zero-loss energy window 10 eV). The overlay shows the radially averaged intensity profile that was used to determine the structure.

(i) determining the unit cell from peak positions; (ii) space-group determination; (iii) extracting structure-factor amplitudes from the intensity profile and solving the structure; (iv) refining the structure model.

3.1. Peak search and unit-cell determination with integrated data

Analysis of the integrated intensity profile (Fig. 2*a*) by means of the peak-search tool implemented in the program *WinPLOTR* (Roisnel & Rodriguez-Carvajal, 2000) yielded 12 peaks between 0.53 and 2.09° 2Θ. The use of the corresponding non-integrated data yielded only the first nine reflections in this 2Θ range. The obtained peak positions were used as input for the program *INDEX* (Stoe & Cie, Darmstadt, Germany), which uses the strategy of the program

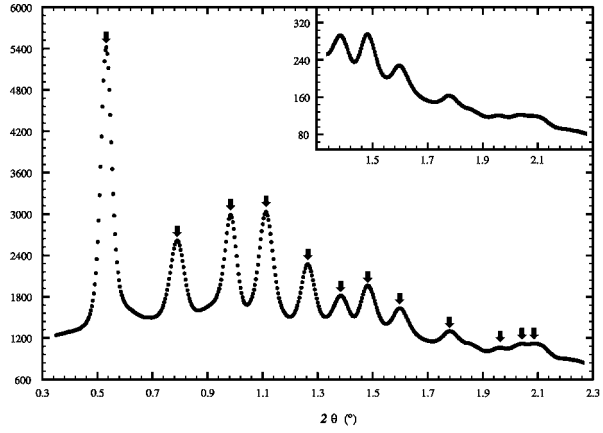

(*a*)

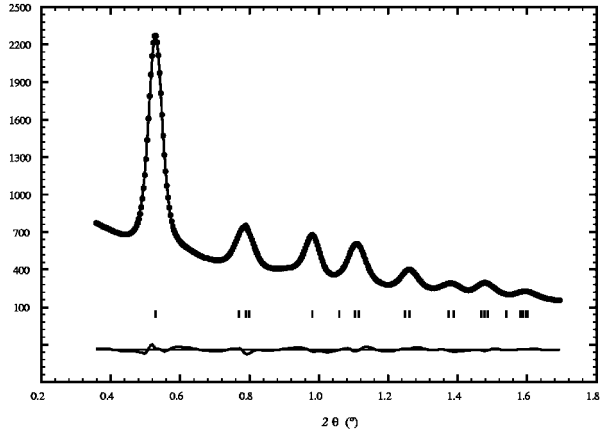

(*b*)

Figure 2
(*a*) Profile of the radially integrated electron powder diagram, which was used in the course of determining the unit cell and for solving the structure by direct methods. Peak positions that have been used for indexing the diagram are indicated by arrows. Comparison with the radially averaged (non-integrated) profile in the inset shows that the peaks at higher angles are substantially enhanced. (*b*) Conventional (radially averaged) intensity profile used for Rietveld refinement. The positions of the Bragg reflections are indicated by vertical bars (|). The deviations between the observed and the calculated intensities from the refined model are shown in the difference plot in the lower part of the diagram (dots = observed intensities; solid line = calculated intensities).

Table 1
Most probable unit cells as suggested by the *TREOR* indexing strategy (radially integrated data).

Used solutions are indicated by * (see text). The row labeled FOM shows the figure of merit of the corresponding solution as defined by de Wolff (1968).

No.	Symmetry	*a*	*c*	Volume	FOM
1	Hexagonal	8.247	1.933	113.8	5.8
2	Hexagonal	8.248	5.794	341.3	3.5
3	Hexagonal	8.248	3.863	227.6	3.3
4	Hexagonal	8.333	4.383	263.5	3.3
5	Hexagonal	8.248	5.299	312.1	3.2
6	*Tetragonal	3.846	9.622	142.3	4.2
7	Tetragonal	8.610	4.410	326.9	3.8
8	*Tetragonal	5.439	9.622	284.6	3.4
9	*Tetragonal	3.875	9.205	138.2	3.3
10	*Tetragonal	5.330	9.622	273.3	3.0

Table 2
Peak list for tetragonal solution No. 6 as obtained from the *TREOR* indexing strategy, $a = 3.846$, $c = 9.622$ Å, $V = 142.3$ Å^3 ($\lambda_{120} = 0.0335$ Å).

2Θ(obs.) (°)	*h*	*k*	*l*	2Θ(calc.) (°)	2Θ(obs.−calc.) (°)	*d*(obs.)	*d*(calc.)
0.532	1	0	1	0.532	0.0000	3.5713	3.5713
0.790	0	0	4	0.790	0.0000	2.4054	2.4055
0.984	0	0	5	0.987	−0.0036	1.9314	1.9244
1.112	2	1	0	1.105	0.0076	1.7083	1.7200
1.264	2	0	4	1.265	−0.0015	1.5038	1.5020
1.384	0	0	7	1.382	0.0015	1.3731	1.3746
1.482	2	1	5	1.482	0.0001	1.2824	1.2824
1.599	3	0	3	1.596	0.0023	1.1887	1.1904
1.780	3	0	5	1.781	−0.0014	1.0678	1.0669
1.963	3	1	6	1.961	0.0020	0.9680	0.9691
2.043	4	1	1	2.047	−0.0035	0.9301	0.9284
2.088	3	1	7	2.086	0.0011	0.9104	0.9109

TREOR (Werner *et al.*, 1985) for finding appropriate unit cells. Part of the output, which shows the ten most probable solutions suggested by the program is shown in Table 1. Since the chemical composition of the material under investigation was known and the fact that MO_2-type transition-metal oxides have a space filling of about 11 Å^3 per atom allowed the use of density calculations to rule out improbable unit cells from the list. Meaningful results were obtained only for hexagonal cell No. 1 ($D_{cal} = 3.5$ g cm^{-3}, $Z = 3$) and the tetragonal cells No. 6 ($D_{cal} = 3.7$ g cm^{-3}, $Z = 4$) and No. 9 ($D_{cal} = 3.8$ g cm^{-3}, $Z = 4$). The unusual short crystal axis of solution No. 1 made this cell rather unlikely, thus only the tetragonal solutions were examined in detail. Closer inspection of the obtained solutions shows that the indexing for No. 6 and No. 9 is consistent with a body-centered cell while the solutions Nos. 8 and 10 suggest a face-centered cell. The *I* cell and the twice as large *F* cell are related by $a_F = a_I \times 2^{1/2}$. The *c* axis remains unchanged in these cases. However, the body-centered cell was chosen as the correct solution since it represents the conventional unit-cell setting. The output for the solution with the highest figure of merit (No. 6) is listed in detail in Table 2.

3.2. Space group

Determination of the most likely space groups was achieved as follows. Although the result from unit-cell determination already suggested a body-centered space group, theoretical line positions were calculated for all 68 tetragonal space groups with lattice parameters from unit cell No. 6. All space groups that permitted peaks at lower angles than the dominant peak at about 0.53° 2Θ (*d* spacing about 3.57 Å) were ruled out since this peak was assumed as the first reflection. After applying this criterion, the following eight space groups were left: $I4_1$ (80), $I4_1/a$ (88), $P4_12_12$ (92), $P4_32_12$ (96), $I4_122$ (98), $I4_1md$ (109), $I\bar{4}2d$ (122), $I4_1/amd$ (141). Visual comparison of the experimental electron powder pattern with the calculated line diagrams for the above listed space groups made it possible to exclude also the two primitive space groups $P4_12_12$ and $P4_32_12$ since these generated a much higher peak density than observed in the experimental data. Thus, only the six body-centered space groups were taken into account for solving the structure.

3.3. Extracting structure-factor amplitudes from integrated intensities and solving the structure

Squared structure-factor amplitudes $|F_{hkl}|^2$ were extracted from the integrated intensity data with the program *FULL-PROF* (Rodriguez-Carvajal, 2000), which uses the profile-matching approach of Le Bail *et al.* (1988). Lattice parameters, background, peak shape and full peak width at half-maximum were refined before the final extraction of the structure-factor amplitudes was carried out for each of the above body-centered space groups. For modeling the peak shape, a pseudo-Voigt function (Thompson *et al.*, 1987) was chosen. The profile matching yielded in all cases conventional Rietveld *R* factors of $R_p = 10\%$, $R_{wp} = 10\%$ and $R_{exp} = 8\%$. The extracted data (*hkl*, $|F_{hkl}|^2$) together with the refined lattice parameters ($a = 3.850$, $c = 9.602$ Å) were then used as input for the direct-methods program *SIR*97 (Altomare *et al.*, 1999), which was modified with atomic scattering factors for electrons (Jiang & Li, 1984).

Although negative isotropic displacement factors were calculated during normalizing the data – an artifact arising from using integrated intensities – the program succeeded in all cases to find a complete structure with reasonable positions for titanium and oxygen atoms. For comparison, the relatively poor result obtained by direct methods with the non-integrated data is shown in Fig. 3(*a*). The obtained results from direct methods on the integrated data are summarized in Table 3. The corresponding graphical representations of the structures are shown in Fig. 4. Visual comparison of the received trial structures shows that all models have the motif of edge- and vertex-linked O_6 octahedra in common. Atomic positions according to space-group symmetry *P*1 (1) were then calculated for all trial structures. The find-symmetry tool implemented in the program *Materials Studio Visualizer* (Molecular Simulations, MSI) was used to identify missing symmetry elements in the structure and to impose the symmetry constraints according to the detected space group. Since $I4_1/amd$ was found in each case as the space group of

Table 3
Results from *SIR97* with radially integrated data (* = alternative setting).

Space group	Fig.	No. of peaks	*R* factor	Atom	Wyckoff position	*X*	*Y*	*Z*
$I\,4_1$ (80)	4(*a*)	29	0.17	Ti	4(*a*)	0	0	0.8513
				O(1)	4(*a*)	0	0	0.0699
				O(2)	4(*a*)	0	0	0.6471
$I\,4_1/a$ (88)*	4(*b*)	26	0.17	Ti	4(*a*)	0	0.25	0.125
				O	8(*e*)	0	0.25	0.3360
$I\,4_1\,2\,2$ (98)	4(*c*)	24	0.19	Ti	4(*a*)	0	0	0
				O	8(*e*)	0	0	0.2131
$I\,4_1\,m\,d$ (109)	4(*d*)	21	0.18	Ti	4(*a*)	0	0	0.8674
				O(1)	4(*a*)	0	0	0.0969
				O(2)	4(*a*)	0	0	0.6757
$I\,\bar{4}\,2\,d$ (122)	4(*e*)	21	0.20	Ti	4(*a*)	0	0	0
				O	8(*c*)	0	0	0.7861
$I\,4_1/a\,m\,d$ (141)*	4(*f*)	20	0.19	Ti	4(*a*)	0.5	0.75	0.375
				O	8(*e*)	0.5	0.75	0.1598

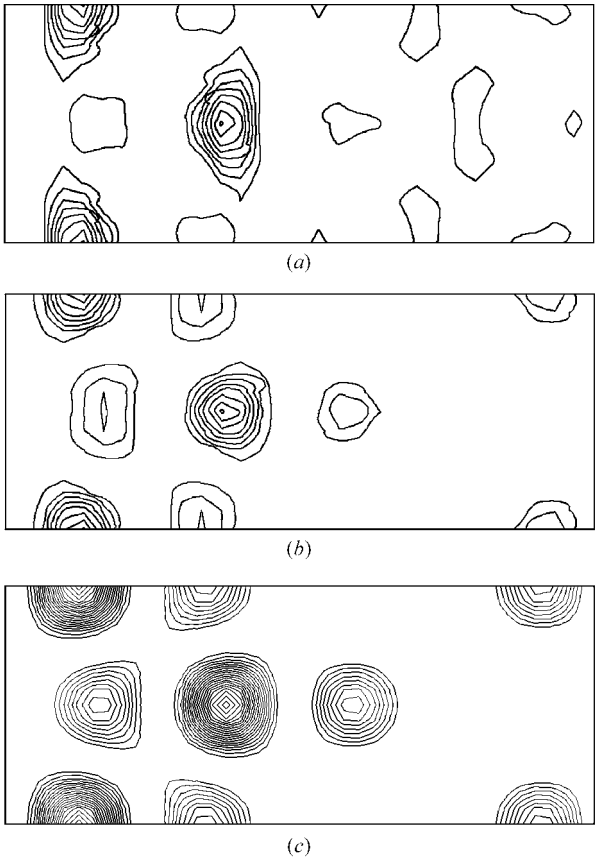

Figure 3
Potential maps for the anatase structure as obtained from the direct-methods program *SIR97* on non-integrated (conventional) data after manual background subtraction (*a*) and on integrated intensities (*b*). The maps show the *ac* section at $y = 0.75$ (space group $I41/amd$, crystallographic resolution about 1.2 Å). Titanium atoms are indicated in the maps by higher potential, oxygen atoms by lower potential. Comparison of the maps in (*a*) and (*b*) shows that integrating the extracted profile has the effect of enhancing the potential of the oxygen atoms relative to the background level. This results in a much 'cleaner' potential map, which allows the atomic positions for oxygen to be detected much more easily. For comparison, the map in (*c*) shows the result after Rietveld refinement with the non-integrated data (origin shift according to the given coordinates in Table 4: $x + \frac{1}{2}$, $z + \frac{1}{4}$).

highest symmetry (maximum deviation 0.016 Å for space group $I4_1$), the corresponding model was assumed as the correct structure solution (Table 4).

3.4. Structure refinement

A final Rietveld refinement (program *FULLPROF*) was carried out with the non-integrated electron powder data for improving the structural parameters of the model. According to common refinement strategies, the first cycles were used to optimize the fit of the background model, for refining the overall scale factor and lattice parameters. Again a pseudo-Voigt function was chosen for modeling the profile of the Bragg reflections. In a subsequent step, the atomic position for oxygen and the isotropic displacement parameters *B* were also refined. Extinction was not taken into account during refinement. The refinement was at all stages stable and yielded

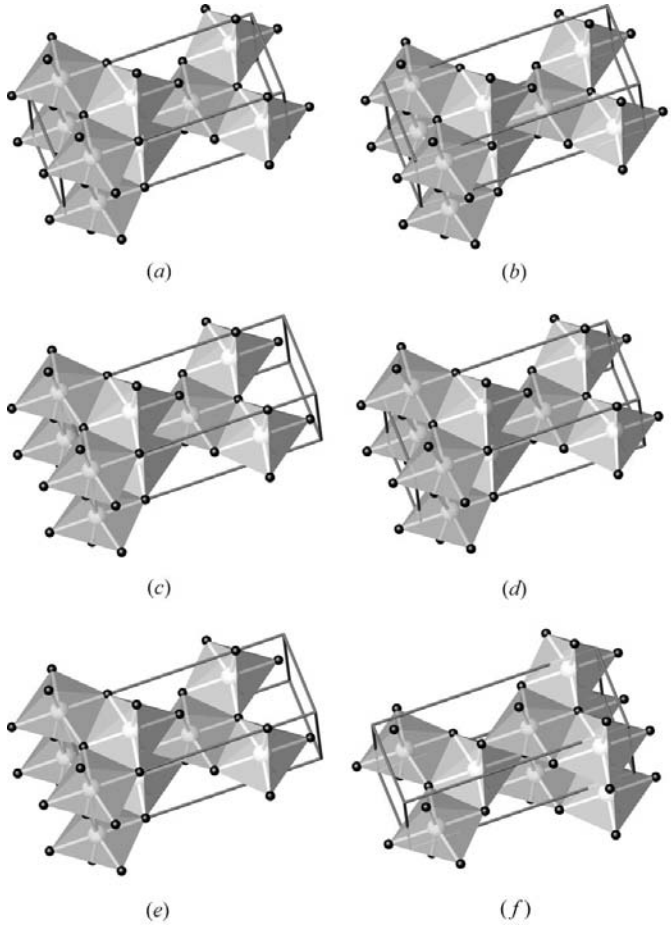

Figure 4
Trial structures as received from the direct-methods program *SIR97* with $|F_{hkl}|^2$ values extracted from the integrated electron powder diffraction data (titanium = large white sphere, oxygen = small black sphere).

Table 4
Results of the structure determination for nanocrystalline anatase using electron powder data.

The results of the structure solution were obtained with radially integrated data. The Rietveld refinement was carried out with radially averaged (non-integrated) data.

Structure solution (integrated I)		
$I\,4_1/a\,m\,d$		
a = 3.850, c = 9.602 Å	Ti (x, y, z):	0.5, 0.75, 0.375
V = 142.3 Å^3	O (x, y, z):	0.5, 0.75, 0.1598
D_{cal} = 3.73 g cm^{-3}		
Rietveld refinement		
a = 3.872 (2), c = 9.616 (5) Å	Ti (x, y, z):	0.5, 0.75, 0.375
V = 144.2 Å^3	O (x, y, z):	0.5, 0.75, 0.1618 (6)
D_{cal} = 3.68 g cm^{-3}	B(Ti):	2.37 (20) Å^2
	B(O):	1.65 (23) Å^2
λ = 0.03317 Å†		
2θ = 0.36–1.7°		
Data points: 366		
Bragg positions: 20		
Q_{max} = 0.7105 Å^{-2}		
Parameters: 15		
$R_{p(conv.)}$ = 6.50%		
$R_{wp(conv)}$ = 6.26%		
$R_{exp(conv)}$ = 12.0%		
R_{Bragg} = 1.69%		
R_F = 1.79%		
GoF = 0.51		

† Corrected according to a Rietveld refinement on a reference pattern of nanocrystalline gold.

within a few iterations the results summarized in Table 4. The oxygen atom was shifted during the whole refinement by less than 0.02 Å from its initial position determined by direct methods. The calculated and the experimental diffraction profiles together with the difference curve obtained after refinement are shown in Fig. 2(*b*). The experimentally obtained structure-factor amplitudes after refinement are listed in Table 5 and compared with the kinematical and dynamical calculated amplitudes.

Table 5
Comparison of extracted experimental structure-factor amplitudes F_{obs} after Rietveld refinement, calculated kinematical amplitudes F_{kin} and calculated dynamical amplitudes F_{dyn}.

The kinematical values F_{kin} were calculated using the refined atom positions with displacement factors set equal to zero. Dynamical amplitudes F_{dyn} were calculated for the exact Laue condition (two-beam case) using the relation (Cowley, 1999; p. 260):

$$F_{dyn} = F_{000}\sin(\lambda F_{kin} t/V).$$

The calculations were carried out for crystallites of mean thickness t = 7 nm. The total scattering power per unit cell is F_{000} = 50.95 Å. The electron wavelength λ and cell volume V were taken from Table 4. The scale factor S in the table below fits the dynamical amplitudes to the kinematical calculated amplitudes and is defined as $S = F_{kin}/F_{dyn}$. The practically constant value for S (mean value 1.208) proves the made assumption of quasi-kinematical scattering for the present investigation. The significant large differences between the kinematical calculated and observed structure-factor amplitudes ($R_{kin-obs}$ = 10.3%) arise mainly from setting the displacement factors for the calculation equal to zero. The R factor is substantially lowered if non-zero displacement factors are used in the calculation, *e.g.* from Rietveld refinement (Table 4). The corresponding R factor is then reduced to 1.9%.

h	k	l	F_{obs}	F_{kin}	F_{dyn}	S
0	2	0	21.19	20.51	16.73	1.226
2	2	0	12.15	14.17	11.68	1.213
0	1	1	18.26	16.12	13.25	1.217
1	2	1	8.07	8.14	6.75	1.206
0	3	1	4.94	5.87	4.87	1.205
1	1	2	3.54	3.72	3.09	1.204
0	2	2	0.00	0.00	0.00	–
1	3	2	0.45	1.27	1.06	1.198
0	1	3	5.05	4.87	4.04	1.205
1	2	3	2.10	2.55	2.12	1.203
0	3	3	1.27	1.92	1.60	1.200
0	0	4	21.66	20.43	16.67	1.226
0	2	4	12.51	12.86	10.61	1.212
2	2	4	8.09	9.64	7.98	1.208
0	1	5	12.47	12.41	10.25	1.211
1	2	5	7.69	8.92	7.39	1.207
1	1	6	5.24	6.32	5.25	1.204
0	2	6	0.00	0.00	0.00	–
0	1	7	0.00	0.55	0.46	1.196
0	0	8	3.65	4.80	3.99	1.203

4. Discussion

The result obtained in the present study shows for the first time that small unit-cell structures of symmetry lower than hexagonal are directly accessible from non-textured electron powder data. The performed structure analysis includes *ab initio* determination of the unit cell, space group and solving and refining the model. Despite this very promising result, several obstacles were encountered at different stages of the structure determination which will be discussed below.

The most formidable problem in any structure determination from powder data is determining the unit cell. Owing to the pronounced intensity decay with increasing scattering angle and the strong overlap of neighboring reflections (see indicated Bragg positions in Fig. 2*b*), it was extremely problematic to extract a reliable set of accurate peak positions from the present electron powder data. These difficulties were notably reduced when the radially integrated intensity profile with substantially enhanced peaks at higher diffraction angles was used for this purpose (Fig. 2*a*). Nevertheless, even if the range of the data could be extended in this way, the peak positions were still ambiguous and as a consequence the indexing program was only able to rule out the cubic system but could not clearly distinguish between the hexagonal and tetragonal systems. Therefore, we faced the difficulty of manually choosing a suitable unit cell from the list of suggested solutions. However, in the present case, we managed to identify the tetragonal cell on the basis of density calculations as described above. In retrospect, it must be said that the knowledge about the approximate density of the material may have been the key information that helped us to arrive in the end at the correct result. It is interesting to note that the prominent tetragonal unit cell could also be found among the highest-ranked solutions when only the first 9 peak positions out of 12 reflections were used, *e.g.* as for the non-integrated data. It was, however, necessary to limit the maximum considered cell volume at 200 Å^3 to get this result. This is of course some pre-information that is usually not available in the course of a structure determination of a real unknown. In cases when automatic (computer) indexing fails,

graphical schemes like Hull–Davey charts (Cullity, 1967) can be helpful to find a proper unit cell. Since such graphs exist only for the hexagonal and tetragonal system, this method cannot be considered as a universal solution for the indexing problem.

Another commonly used approach for determining unit-cell dimensions, Bravais lattice and space group is based on the analysis of electron microdiffraction (Morniroli & Steeds, 1992) or convergent-beam electron diffraction (CBED) patterns (Zuo, 1993; Tanaka, 1994). These techniques could, however, not straightforwardly be applied to the nanocrystalline powder investigated here since non-agglomerated nanocrystals, which could be studied individually, were not present in the sample. Moreover, owing to the shape transform, almost spherical crystallites of 7 nm in diameter will hardly produce sharp higher-order Laue-zone (HOLZ) lines which are indispensable for deriving space-group symmetry from CBED patterns.

The search for suitable space groups was mainly performed on the basis of comparing the experimental and the calculated line diagrams as described above. This was a time-consuming but straightforward procedure that yielded in the end directly the six body-centered space groups. The subsequent extraction of the squared structure-factor amplitudes and finally solving the structure with standard crystallographic software worked also without major problems. As already mentioned, the results obtained by the direct-methods program *SIR97* were much better when radially integrated data were used instead of the conventional non-integrated data. For example, while the potential map calculated for space group $I4_1/amd$ using normalized non-integrated data shows the oxygen peaks at almost the same level as the ghost peaks (Fig. 3*a*), the corresponding map calculated from the integrated data is much *cleaner* and shows all oxygen positions as well defined sharp peaks (Fig. 3*b*). This is a direct result of data treatment since the natural fall off in the atomic scattering factor at larger diffraction angles is to some extent compensated by radially integrating the profile. As a consequence, a larger scattering power is assigned to the atoms than they have in reality. That this procedure is very effective for detecting light atoms in the presence of heavier ones is nicely demonstrated by the present example.

As reported above, Rietveld refinement was applied in the final step with non-integrated data to check and improve the obtained structural model from direct methods. According to previous results from neutron powder diffraction, the oxygen z parameter in the anatase structure can vary between 0.1669 (Burdett *et al.*, 1987) and 0.2081 (Howard *et al.*, 1991). The corresponding models of the two structures are shown in Figs. 6(*a*) and 6(*b*). This range corresponds to an overall shift in the oxygen position of about 0.4 Å. Shifting the oxygen along this distance goes along with pronounced changes in the relative intensities as illustrated by the calculated profiles shown in Fig. 5. The position determined in the present study (z = 0.1618, see Table 4) is somewhat below the above lower limit for coarse-grained material. This value differs only slightly from the recently determined parameter for the same material using integrated (unfiltered) 300 keV electron powder data (z = 0.1656; Weirich *et al.*, 2000). For comparison, a refinement carried out with the integrated data used in this study yields an even lower z parameter of 0.1593. Nevertheless, the deviation in the fractional atomic position for oxygen as determined from neutron powder diffraction (lower limit) and from electron powder diffraction is about 0.008. This value corre-

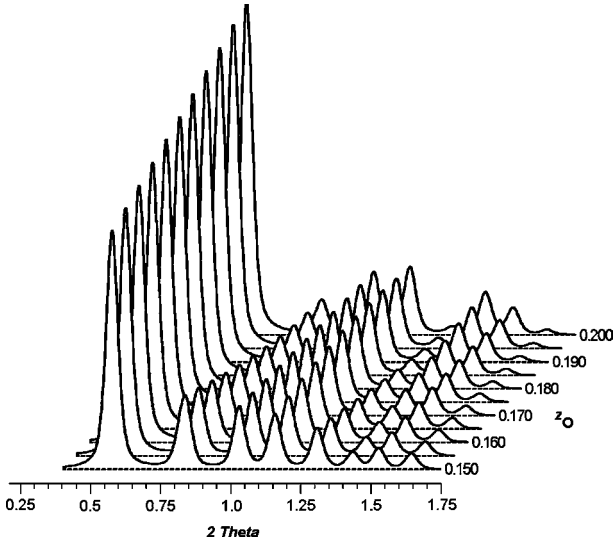

Figure 5
Calculated electron powder diagrams for anatase with varying oxygen positions between z_O = 0.150 and 0.200. The calculation was performed for 120 keV electrons (λ = 0.0335 Å).

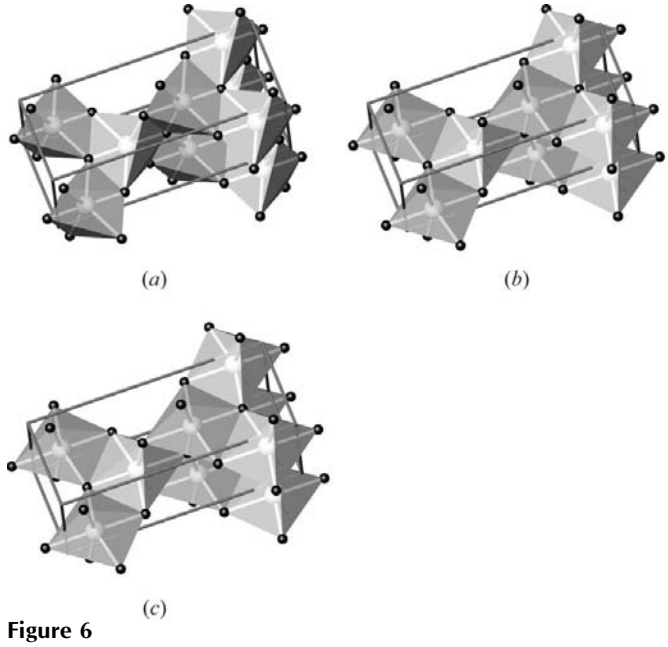

Figure 6
Structures of anatase with varying oxygen position as determined from neutron diffraction by (*a*) Howard *et al.* (1991) [z_O = 0.2081] and (*b*) by Burdett *et al.*, (1987) [z_O = 0.1669]. The structure in (*c*) shows the result of the present study after Rietveld refinement with the electron powder data (z_O = 0.1618). The structures shown in (*b*) and (*c*) are built up of almost regular TiO_6 octahedral units, which suggests reduced internal stress (see text). [Ti = large white spheres, O = small black spheres.]

sponds to a distance of less than 0.08 Å. Although the oxygen position appears to be numerically determinable with a precision of four decimals (see Table 4), it is hard to trust that the refinement carried out with electron powder data from nanocrystalline powders is able to sense such extremely small structural changes. Slight (systematic) deviations from the assumed perfect random orientation distribution of the crystallites as well as (random) effects arising from the size distribution (larger crystallites diffract stronger and make the powder pattern 'spotty', see Fig. 1) can alter the intensity profile and thus slightly change the result of the refinement. In fortunate cases, when just a few larger crystallites contribute at random to the intensities, this effect might be cancelled out and the refined atom positions are simply determined with lower precision. This of course assumes that the main structural parameters (atom positions) are the same for all crystallites in the sample and do not depend on the size of the nanocrystals and that there is not some undescribed physics in the experiment that affects the background and/or the intensities. In order to estimate the real errors of the experiment, it might be necessary for future investigations to repeat the refinement with several data sets from the same sample and compare the results afterwards.

In contrast to samples with pronounced preferred orientation, for which appreciable *n*-beam dynamical diffraction has been reported (Turner & Cowley, 1969; Imamov *et al.*, 1976), non-systematic interactions are assumed to play only a minor role for investigations of the present type, which are based on averaging over all possible crystal orientations (Cowley, 1999). This assumption is also justified since the average crystallite size of 7 nm is less than 1/9 of the shortest calculated extinction distance (about 66 nm for the 020 diffracted beam). Accordingly, the two-beam dynamical amplitudes, which have been calculated as a rough estimate to check the amount of dynamical diffraction, and the kinematical amplitudes were found identical (see Table 5). However, it can be suspected that weak dynamical diffraction effects might have affected the result since the refined displacement factors that have been determined are somewhat larger for titanium than for oxygen (Table 4). On the other hand, this can also be interpreted in terms of a slight disorder in the titanium framework, a likely feature for nanocrystalline materials with a large number of near-surface atoms that are not necessarily as well ordered as in the regular lattice. Moreover, a non-optimum modeling of the background can also lead to errors, which might result in wrongly determined displacement factors. In accordance with the above discussed result, the oxygen-to-titanium potential ratio in the potential map is measured somewhat higher for the refined structure ($\varphi_O/\varphi_{Ti} = 0.44$) than calculated with atoms at rest ($\varphi_O/\varphi_{Ti} = 0.375$). Since this disagreement is not very large, it seems permissible to assume that any errors in the data may have preferentially affected the displacement factors and thus the refined positions represent, with some experimental error, the true mean position of the atoms within the unit cell. However, even if the real accuracy of the determined oxygen position is perhaps lower than the numerical precision given in the output of the refinement program, the overall result appears quite plausible. This can be readily checked by comparing the experimental and calculated intensity profiles (Figs. 2*b* and 5). The obtained result seems also reasonable from the structural point of view since nanocrystalline materials are expected to form the most 'relaxed', *i.e.* stress-free, structures. Comparison of the structures from neutron powder diffraction (Fig. 6*b*) with the one obtained in the present study (Fig. 6*c*) clearly supports this hypothesis. The effect of reduced stress in the nanocrystals is possibly also expressed in a reduced density (about 3.7 g cm^{-3}, Table 4) if compared with bulk material [about 3.9 g cm^{-3} (Howard *et al.*, 1991; Burdett *et al.*, 1987)]. Whether this difference is characteristic for the investigated material or if this is an artefact caused by calibration errors (*e.g.* slightly different camera length) is difficult to judge at the present stage since the refinement was not carried out with an internal standard. Thus at least a second data set containing reflections from the material under investigation and reflections from a material with known lattice parameters are needed if high accuracy of the refined unit-cell parameters is required. However, despite some uncertainties concerning the exact unit-cell dimensions, the calculated shortest atom distances for the refined structure (Ti—O = 1.968 and 2.050, Ti—Ti = 3.088 Å) agree within less than 3.6% with those determined by Burdett *et al.* (Ti—O = 1.934 and 1.979, Ti—Ti = 3.039 Å).

Finally, some remarks on the *R* values of the refinement seem advisable. Although the fit of the calculated pattern to the observed data is nearly perfect as seen by the almost flat difference curve (Fig. 2*b*), some of the residuals listed in Table 4 indicate non-optimum data. In particular, the weighted-profile *R* value R_{wp}, the expected *R* value R_{exp} and accordingly also the goodness-of-fit factor (GoF) account for the high background (from incoherent scattering) and the relatively poor counting statistics. Nevertheless, according to McCusker *et. al.* (1999), a good fit between the observed and calculated profile and a meaningful structure model are the most important criteria for a good-quality Rietveld refinement. Both of these criteria are certainly met by the present refinement results.

5. Conclusions

The outcome of the present study proves that electron powder data of non-textured nanocrystalline materials contain sufficient information for determining crystal structures from scratch. However, as shown for the present example, there are sometimes several complications before this goal is reached. The encountered difficulties in finding the correct unit cell and space group are the same as known for the corresponding approach based on X-rays (Cheetham, 1995; Harris & Tremayne, 1996). In particular, for successfully determining the correct unit cell, it is mandatory to obtain a rather large set of accurate peak positions, which is not an easy task owing to the broadened and heavily overlapping peaks from tiny crystallites. Moreover, it was shown by theoretical calculations that dynamical diffraction effects, which are often feared to

threaten the validity of the used quasi-kinematical approach, could be neglected in the present case.

In summary, one can state that electron powder diffraction of texture-free nanocrystalline materials is in principle capable of providing atom positions of reasonable accuracy and precise lattice parameters. Even with the discussed inherent drawbacks of the powder method in mind, electron powder diffraction has great potential to overcome the present limitations of X-ray crystallography for studying the interior structure of nanocrystalline materials and thin films that often exist in only extremely small quantities.

We thank Dipl.-Ing. Kersten Hahn (Max-Planck Institut für Metallforschung, Stuttgart, Germany) for technical support during data acquisition on the Zeiss EM912 microscope. Molecular Simulations Inc. is acknowledged for a trial copy of the *Materials Studio* program.

References

Albinati, A. & Willis, T. M. (1999). *International Tables for Crystallography*, Vol. C, *Mathematical, Physical and Chemical Tables*, edited by A. J. C. Wilson & E. Prince, pp. 704–705. Dordrecht: Kluwer Academic Publishers.

Altomare, A., Burla, M. C., Camalli, M., Cascarano, G., Giacovazzo, C., Guagliardi, A., Moliterni, A. G. G., Polidori, G. & Spagna, R. (1999). *J. Appl. Cryst.* **32**, 115–118.

Burdett, J. K., Hughbanks, T., Miller, G. J., Richardson, J. W. & Smith, J. V. (1987). *J. Am. Chem. Soc.* **109**, 3639–3646.

Cheetham, A. K. (1995). *The Rietveld Method*, edited by R. A. Young, pp. 276–292. Oxford University Press.

Cowley, J. M. (1968). *Prog. Mater. Sci.* **13**, 269–321.

Cowley, J. M. (1999). *International Tables for Crystallography*, Vol. C, *Mathematical, Physical and Chemical Tables*, edited by A. J. C. Wilson & E. Prince, pp. 80–82, 259–262. Dordrecht: Kluwer Academic Publishers.

Cullity, B. D. (1967). *Elements of X-ray Diffraction*, 3rd reprint, ch. 10. New York: Addison-Wesley.

Dorset, D. L. (1995). *Structural Electron Crystallography*. New York: Plenum Press.

Giacovazzo, C. (1996). *Acta Cryst.* A**52**, 331–339.

Harris, K. D. M. & Tremayne, M. (1996). *Chem. Mater.* **8**, 2554–2570.

Howard, C. J., Sabine, T. M. & Dickson, F. (1991). *Acta Cryst.* B**47**, 462–468.

Imamov, R. M., Pannkhorst, V., Avilov, A. S. & Pinsker, Z. G. (1976). *Sov. Phys. Crystallogr.* **21**, 199–202.

Jiang, J. S. & Li, F. H. (1984). *Acta Phys. Sin.* **33**, 845–849.

Le Bail, A., Duroy, H. & Fourquet, J. L. (1988). *Mater. Res. Bull.* **23**, 447.

McCusker, L. B., Von Dreele, R. B., Cox, D. E., Louer, D. & Scardi, P. (1999). *J. Appl. Cryst.* **32**, 36–50.

Morniroli, J. P. & Steeds, J. W. (1992). *Ultramicroscopy*, **45**, 219–239.

Pinsker, Z. G. (1953). *Electron Diffraction.* London: Butterworths.

Rodriguez-Carvajal, J. (2000). *FULLPROF, a Program for Rietveld, Profile Matching and Integrated Intensities Refinement of X-ray and/or Neutron Data.* Laboratoire Leon Brillouin, CEA-Saclay, France.

Roisnel, T. & Rodriguez-Carvajal, J. (2000). *WinPLOTR, a New Tool for Powder Diffraction.* Laboratoire Leon Brillouin, CEA-Saclay, France.

Seifried, S., Winterer, M. & Hahn, H. (2000). *Chem. Vap. Dep.* **6**, 239–244.

Tanaka, M. (1994). *Acta Cryst.* A**50**, 261–286.

Thompson, P., Cox, D. E. & Hastings, J. B. (1987). *J. Appl. Cryst.* **20**, 79–83.

Thomson, G. P. & Reid, A. (1927). *Nature (London)*, **119**, 890.

Turner, P. S. & Cowley, J. M. (1969). *Acta Cryst.* A**25**, 475–481.

Vainshtein, B. K. (1964). *Structure Analysis by Electron Diffraction.* Oxford: Pergamon Press.

Vainshtein, B. K., Zvyagin, B. B. & Avilov, A. S. (1992). *Electron Diffraction Techniques*, Vol. 1, edited by J. M. Cowley, pp. 216–312. Oxford University Press.

Weirich, T. E., Winterer, M., Seifried, S., Hahn, H. & Fuess, H. (2000). *Ultramicroscopy*, **81**, 263–270.

Werner, P. E., Eriksson, L. & Westdahl, M. (1985). *J. Appl. Cryst.* **18**, 367–370.

Wolff, P. M. de (1968). *J. Appl. Cryst.* **1**, 108–113.

Young, R. A. (1995). Editor. *The Rietveld Method.* Oxford University Press.

Zuo, J. M. (1993). *Ultramicroscopy*, **52**, 459–464.

Zou, X. D., Weirich, T. E. & Hovmöller, S. (2000). *Progress in Transmission Electron Microscopy*, Vol. 1, edited by X. F. Zhang & Z. Zhang, pp. 223–259. Berlin: Springer Verlag.

Zvyagin, B. B. (1967). *Electron Diffraction Analysis of Clay Mineral Structures.* New York: Plenum Press.

Zvyagin, B. B. (1999). *International Tables for Crystallography*, Vol. C, *Mathematical, Physical and Chemical Tables*, edited by A. J. C. Wilson & E. Prince, pp. 708–710. Dordrecht: Kluwer Academic Publishers.